Effects of Density Ratio on Rotary Jet Flow Induction

J. D. McBrayer*
Parks College of Aeronautical Technology, Cahokia, Ill.

AND

K. H. Hohenemser†
Washington University, St. Louis, Mo.

Rotary jet flow induction has been considered as a simple means of jet thrust augmentation for VTOL aircraft or other jet propelled vehicles. In potential applications, the primary gas, when expanded to ambient pressure, usually has lower density than the secondary air with which it interacts. Previous analysis has indicated improvements in flow induction for low primary to secondary gas density ratios, however no substantiating tests were available. The present study fills this gap. Experiments have been conducted with a rotary jet device using as the secondary medium ambient air and as the primary medium either helium, a helium-nitrogen mixture, or air, thus covering a range of primary to secondary flow density ratios from 1:7 to 1:1. Substantially smaller improvements of secondary flow induction with lower primary gas density were found than could be predicted with the previous analysis. A revised analysis was correlated with the test results and indicated that with lower primary gas density increasing flow mixing must occur before the process of mutual flow deflection takes place, thereby reducing the effectiveness of rotary jet flow induction for low primary to secondary flow density ratio. Optimum thrust augmentation is obtained for density ratios of about 1:3.

Nomenclature

A = flow area
l = distance of primary jet travel
P = pressure
r = radial distance from rotor axis
T = absolute temperature
u = velocity in the rotating frame of reference
v = velocity in the inertial frame of reference
$\dot{W}$ = mass flow rate
α = coning angle, as defined in Fig. 1
β = effective spin angle, angle between generatrix of the cone and the direction of the primary jet (rotor fixed frame of reference), as defined in Fig. 1
λ = entrainment coefficient, relative mass flow increment of primary jet per unit length
ρ = density
ϕ = thrust agumentation ratio

Subscripts and superscripts

e = end of interaction duct
i = inlet
p = primary
s = secondary
t = tangential
$'$ = state variable after isentropic expansion from inlet state to static pressure at exit station
0 = stagnation condition
$-$ = nondimensional quantities referred to primary gas condition after isentropic expansion to exit pressure

Introduction

THE use of jet flow induction methods is attractive in jet pumps or jet thrust augmentors if simplicity and low weight of the device are more important than high efficiency. The most common flow induction device is the ejector where the energy and momentum transfer between flows is primarily accomplished by turbulent shear layers. The ejector requires a low static pressure in the mixing zone[1] and long mixing ducts[2] in order to achieve reasonable efficiency. In a second method of flow induction, the primary gas is discharged in the form of pulses, thereby stacking secondary and primary flow segments in the interaction duct. With this arrangement, the flow pattern is nonstationary and compression and expansion waves travel inside the interaction duct. A third method also makes use of stacking primary and secondary flow within a duct, however, wave generation is avoided by producing a flow pattern that is stationary in a rotating frame of reference. This is accomplished by primary jet nozzles rotating about the axis of the interaction duct, as shown in Fig. 1. The rotary jet flow inductor was analyzed by Foa[3] and with an improved method by Hohenemser and Porter,[4] who also correlated the analysis with experimental data on air to air rotary jet inductors and who predicted substantial improvements for low-density primary media, for example helium to air rotary jet inductors. Test results on steam to water rotary jet inductors were presented by Sarro and Avellone.[5] Because of condensation phenomena, the analytical methods developed so far are believed to be inapplicable to steam-water interaction. Two conclusions can be drawn

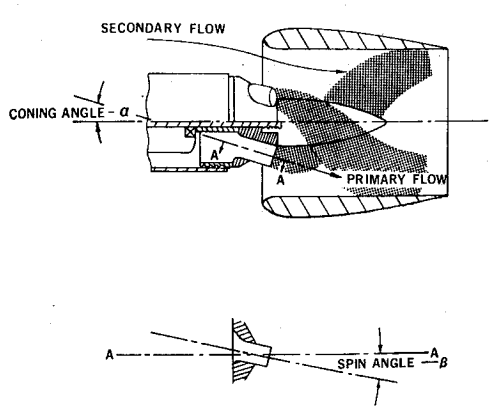

Fig. 1 Rotary jet flow inductor.

Received May 20, 1969; revision received October 1, 1969. This paper is based on the doctoral dissertation prepared by the first author under the direction of the second author.

* Associate Dean and Associate Professor, Department of Aerospace Engineering; also Consultant, Emerson Electric Company. Member AIAA.

† Professor, Department of Aerospace Engineering. Associate Fellow AIAA.

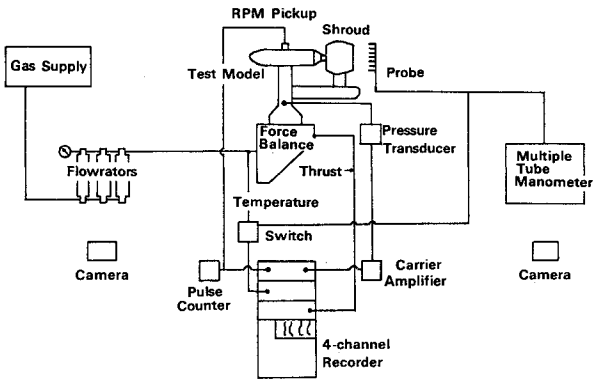

Fig. 2 Schematic diagram of equipment.

from the past studies: the rotary jet flow inductor is more efficient than an ejector of equal duct cross section and it requires a shorter interaction duct.

The tests to be discussed in this paper were conducted in order to check the validity of the analysis by Hohenemser and Porter[4] for low primary to secondary gas density ratios. This was accomplished by using as secondary medium ambient air and as primary medium either helium, a helium-nitrogen mixture, or air, so that a range of primary to secondary flow density ratios of 1:7 to 1:1 was covered. These density ratios refer to gas conditions at ambient pressure. A revision to the analysis which was necessary in order to obtain satisfactory correlation over the entire density ratio range is also discussed in this paper.

Experimental Apparatus

A schematic of the test set-up is given in Fig. 2. The test model consists of 1) a streamlined upright duct to which the hub forebody and a shroud slide mount are attached; 2) the bearing mount assembly; 3) the rotor and labyrinth seal; 4) the nozzle hub and after body; 5) an axially adjustable shroud. Figure 3 is a photograph of the model illustrating the various components.

Five different nozzle hubs were used, each having three nozzle inserts set at a coning angle of 15°. The total nozzle flow area of each hub is 0.284 in^2. The nozzle hubs have geometric spin angles, i.e., that angle to the hub centerline when viewed in a tangential plane, of 0°, 6°, 9°, 14°, and 20°. Figure 1 illustrates the nozzle hub geometry and defines the coning angle and the spin angle. Two different shrouds were used during the air tests. Both shrouds have an inside diameter of 2.42 in.; shroud lengths are 2.38 and 3.10 in.

All primary gas was supplied from storage vessels; therefore, test time was limited to approximately 10–20 sec/run. Air was supplied from two manifolded high-pressure spheres. Helium and the helium-nitrogen mixture were supplied from standard high-pressure gas cylinders through a ten bottle (maximum) manifold. The inducted secondary flow consisted of ambient air.

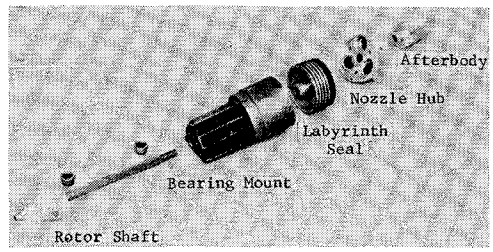

Fig. 3 Photograph of the test model.

A listing of the ranges of experimental parameters investigated is given in Table 1. The measured primary pick-up pressure was corrected for pressure losses between the location of the pressure transducer and the primary gas nozzles. These pressure losses were determined from flow tests with a calibration nozzle. The measured primary flow rate was corrected for leakage flow through the labyrinth seal of the nozzle rotor, determined from tests with blocked nozzles. The leakage flow varied within the test range from 3 to 6% of the nozzle flow. The total mass flow was measured directly by a Pitot-static pressure profile at the shroud exit. Using a one-dimensional flow model, the total mass flow could also be determined from the thrust measurement. The results of both methods agreed to within a few percent. Total primary temperature was measured in the vertical duct and no corrections for the total temperature of the nozzles were required. Nozzle rotor rpm was measured by an electromagnetic pick up and displayed digitally by an electronic counter. Thrust was measured by a strain gauge balance system and no correction from the effects of the flexible pressure line was required.

Because of nozzle rotor drag and misalignments of the emerging primary jets with the nozzle axes, produced by Coanda effects, the effective spin angle defined by $\tan\beta = v_t/v_p$, with v_t measured in the nozzle exit center, is smaller than the geometric spin angle listed in Table 1. The test results of Figs. 7–9 are plotted vs the effective rather than the geometric spin angle.

Results of Previous Analysis

The most refined of the existing analytical flow models was that of Hohenemser and Porter.[4] In this analysis, which is based on the strip concept, the primary and secondary flows are assumed to undergo a mutual flow deflection in a ring-shaped interaction region of finite thickness and curvature. The actual flow pattern during this deflection is not defined. The assumption made is that after completion of this mutual deflection the secondary flow velocity in each elementary ring layer is uniform and has, in the rotor fixed reference system, the same direction β as the primary jet velocity. The mutual flow deflection process in each layer is assumed to be isentropic. Entrainment mixing occurs after the mutual flow deflection in a layer and prior to the flow interaction in the adjoining layer. The primary jet mass is therefore increased while the mass of the secondary flow is de-

Table 1 Test parameters

Primary gas composition	ρ air[a] / ρ test gas	Geometric spin angle	Pickup pressure	Shroud configuration
Air	1.0	0°, 6°, 9°, 14°, 20° Calibration nozzle	0–40 psig	No shroud Short shroud Long shroud
Helium-nitrogen mixture	2.76	0°, 6°, 9°, 14°, 20° Calibration nozzle	0–30 psig	No shroud Short shroud
Helium	7.2	0°, 6°, 9°, 14° Calibration nozzle	0–47 psig	No shroud Short shroud

[a] Measured at standard temperature and pressure.

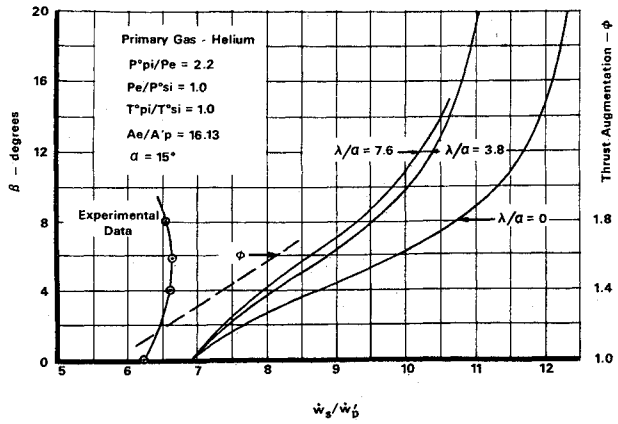

Fig. 4 Effect of entrainment coefficient—analytical flow model of Ref. 4.

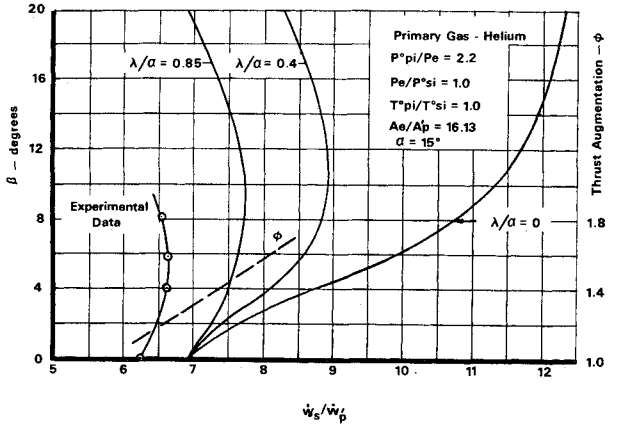

Fig. 6 Effect of entrainment coefficient—new analytical flow model.

creased. Following this mutual flow deflection, a constant area mixing phase is added. Thus, for a nonspinning rotor ($\beta = 0°$), this analysis reduces to the case of the ideal constant area ejector. Correlation of the analytical with test results is achieved by proper selection of an entrainment coefficient λ.

The equations of Ref. 4 have been solved numerically on a digital computer for the following conditions:

Primary Gas		Helium	
$P_{pi}°/P_e$	= 2.2	α	= 15°
$T_{pi}°/T_{si}°$	= 1.0	$\bar{r}_n$	= 1.0
A_e/A_p'	= 16.13	λ/α	= 0, 3.8, 7.6

Figure 4 illustrates the variation of the mass flow ratio with the spin angle as determined from this analysis. Also shown on this figure is the variation of the thrust augmentation ratio with the mass flow ratio. It should be noted that the thrust augmentation variation with mass flow is independent of the entrainment coefficient. Some of the helium test results are also included on this plot for comparison purposes.

The effect of an increase in the entrainment coefficient can be seen in Fig. 4 as a reduction in the mass flow ratio for a given (nonzero) spin angle. For values of the entrainment coefficient λ/α of over 4, this effect rapidly approaches an asymptotic value indicating that the analysis is not capable of reasonable correlation with the helium test data. However, in the case of air as the primary and secondary fluids, as shown in Ref. 4 and substantiated in Ref. 6, a reasonable correlation between the analysis and the test data are possible.

Revised Analytical Model

As stated previously, the analysis of Hohenemser and Porter[4] assumes that in each ring layer postulated in the strip concept the primary and secondary flows first experience a mutual isentropic deflection into a common direction and then are subject to a certain amount of entrainment mixing before the augmented primary jet interacts with the secondary flow of the subsequent layer. Since this type of analysis, as shown in Fig. 4, fails to provide satisfactory correlation with the helium tests, it becomes necessary to revise the analytical flow model. For this purpose, it is helpful to examine the

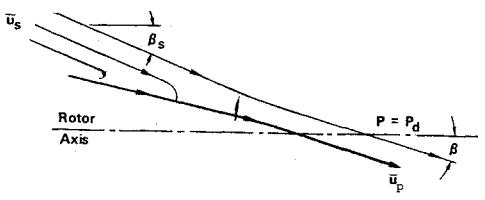

Fig. 5 Schematic interaction flow pattern in rotor-fixed reference frame.

interaction flow pattern shown schematically in Fig. 5 using a rotating frame of reference. This steady-state flow pattern is a planar representation of the flow within a thin cylindrical ring between the centerbody and the duct of the rotary jet flow inductor. The primary flow approaches the deflection region at an oblique angle to the rotor axis. The secondary flow enters this region at a larger oblique angle because the secondary axial velocity is less than the primary axial velocity. The primary and secondary tangential velocities must be equal. The two flows undergo a "glancing collision" and exit the deflection region having a common flow direction.

In the preceding flow models by Foa[3] and Hohenemser and Porter,[4] it was assumed that no flow mixing occurs prior to the mutual flow deflection into a common direction. The entrainment process postulated in Ref. 4 is characterized by the linear momentum equation for the direction of $\bar{u}_p$.

$$\overline{W}_p\bar{u}_p + \Delta\overline{W}_p\bar{u}_s = (\overline{W}_p + \Delta\overline{W}_p)(\bar{u}_p + \Delta\bar{u}_p) \qquad (1)$$

The left hand side refers to the conditions before entrainment of the flow increment $\Delta\overline{W}_p$ and the right hand side to the condition after entrainment. The flow increment $\Delta\overline{W}_p$ was assumed to be proportional to the length element Δl of the primary jet:

$$\Delta\overline{W}_p = \lambda\Delta l = \lambda\Delta r/\alpha\cos\beta \qquad (2)$$

λ being the entrainment coefficient.

Because of the existence of a stagnation region in the secondary flow (see Fig. 5), it is clear that at least some of the secondary flow will join the primary jet before being deflected. One could consider superimposing this type of mixing prior to flow deflection with the mixing after flow deflection postulated in the original analysis. This superposition would, however, introduce two additional empirical parameters into the analysis, one more entrainment factor and one mass flow ratio factor. In order to avoid more than one empirical coefficient in the analysis, it was tentatively assumed that λ refers only to entrainment before flow deflection and that there is no entrainment mixing in a secondary flow layer after flow deflection. As will be seen later, satisfactory correlation of all of the current test data, including the helium tests, is obtained with the modified analysis. The success of the correlation should not be interpreted as a confirmation of the underlying flow entrainment concept, which most likely is an oversimplification of the actual flow.

In the modified analysis Eq. (2) is used with a different interpretation of the entrainment coefficient λ and in conjunction with the modified momentum equation

$$\overline{W}_p(\bar{u}_p\cos\beta) + (\bar{u}_s^2 - \bar{v}_t^2)^{1/2}\Delta\overline{W}_p = (\overline{W}_p + \Delta\overline{W}_p)[\bar{u}_p\cos\beta + \Delta(u_p\cos\beta)] \qquad (3)$$

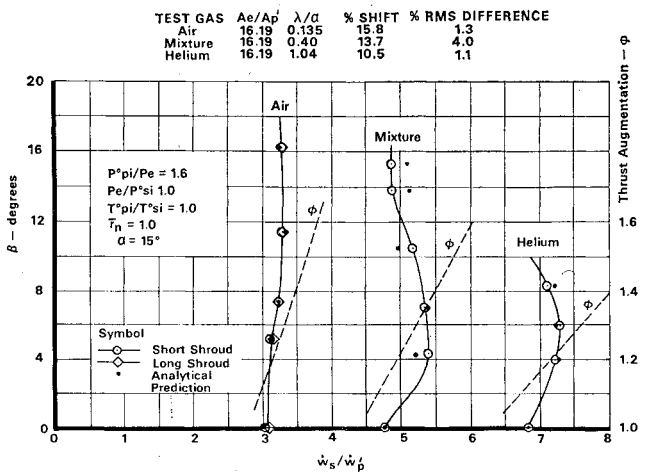

Fig. 7 Comparison of the analytical prediction with the experimental variation, pressure ratio = 1.6.

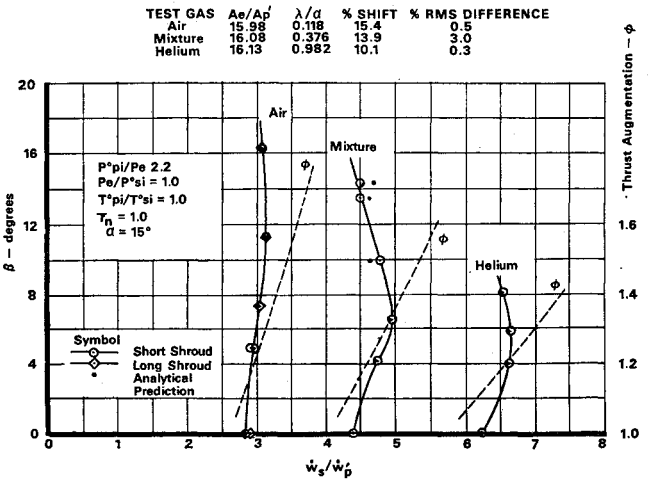

Fig. 8 Comparison of the analytical prediction with the experimental variation, pressure ratio = 2.2.

which expresses entrainment of secondary flow into the primary flow before the mutual flow deflection. Neglecting higher-order small terms Eq. (3) is equivalent to the differential equation

$$\partial(\bar{u}_p \cos\beta)/\partial\bar{\dot{W}}_p = -[(\bar{u}_p \cos\beta) - (\bar{u}_s^2 - \bar{v}_t^2)^{1/2}]/\bar{\dot{W}}_p \quad (4)$$

Since

$$\partial(\bar{u}_p \cos\beta)/\partial\bar{r} = 0 \quad (5)$$

the total differential change of the primary axial velocity component with radius becomes, after insertion of Eq. (2)

$$d(\bar{u}_p \cos\beta)/d\bar{r} =$$

$$-\lambda[(\bar{u}_p \cos\beta) - (\bar{u}_s^2 - \bar{v}_t^2)^{1/2}]/(\bar{\dot{W}}_p \alpha \cos\beta) \quad (6)$$

Performing the differentiation on the left-hand side and rearranging terms:

$$d\bar{u}_p/d\bar{r} = -(\bar{u}_p/\cos\beta)d(\cos\beta)/dr -$$

$$\lambda[\bar{u}_p - (\bar{u}_s^2 - \bar{v}_t)^{1/2}/\cos\beta]/(\bar{\dot{W}}_p \alpha \cos\beta) \quad (7)$$

For zero entrainment $\lambda = 0$, the modified analysis is identical to the analysis of Hohenemser and Porter.[4] Equation (7) is therefore, for $\lambda = 0$, identical to Eq. (16) in Ref. 4, while for nonzero λ the factor $\bar{u}_p - (\bar{u}_s^2 - \bar{v}_t^2)^{1/2}/\cos\beta$ of Eq. (7) replaces the factor $(\bar{u}_p - \bar{u}_s)$ in Eq. (16) of Ref. 4. Otherwise the analysis remains the same, except that because of a typographical error the factor $\bar{c}_{ps}$ was omitted on the right-hand side of Eq. (28) in Ref. 4.

Results of the Revised Analysis and Comparison with Tests

The equations for the revised mathematical flow model were solved numerically for the same case solved previously, and the results are plotted in Fig. 6. For $\lambda/\alpha = 0$, the variation of the effective spin angle β with mass flow is the same in Figs. 4 and 6. Similarly, since the thrust augmentation vs mass flow ratio is independent of entrainment, the ϕ curve is the same in Figs. 4 and 6.

The differences because of the mixing models are quite apparent, however. With the new mixing model, the mass flow ratio decreases quite rapidly with increasing entrainment mixing. Indeed, the mass flow is shown to be reduced almost 50% at $\beta = 20°$ with an entrainment coefficient of 0.22 ($\lambda/\alpha = 0.85$), while for the previous analysis, an entrainment coefficient of 1.99 ($\lambda/\alpha = 7.6$), produced only about a 10% reduction.

A comparison between the experimental and analytical variations in the effective spin angle with mass flow implies that the new mixing model should be capable of closely describing the trend of the variation, given the proper value for the entrainment coefficient.

Three test series were utilized in the comparison between analytical and experimental results: tests with air, a helium-nitrogen mixture, and helium as the primary gas. Details of the tests are described in Ref. 6. Summary curves are given in Figs. 7–9 for the variation of the mass flow ratio, $\dot{W}_s/\dot{W}'_p$ with the effective spin angle β. The total pressure ratios represented on these figures are 1.6, 2.2, and 2.8, respectively. On each of the figures the mass flow-spin angle variations are given for the three primary gases investigated, i.e., for air, for the helium-nitrogen mixture, and for helium. In addition, the analytical variation of the augmentation ratio ϕ with the mass flow ratio is illustrated. The experimental data have been plotted using the effective spin angle, as determined from the spin rate and hub geometry, and the measured augmentation ratio, defined as the experimental thrust divided by the experimental thrust with the zero spin angle hub and no shroud. The analytical results are shown as points at the same spin angle as the experimental values.

In addition to selecting for the analysis a value of λ for the entrainment coefficient which best correlates with a particular test series at given primary pressure ratio and at given density ratio, the analytical mass flow ratios for a test series were also reduced by a constant percent mass flow deficiency, which accounts for friction and flow nonuniformity losses not considered in the analysis. The percent mass flow deficiency as function of density ratio and pressure ratio is shown in Fig. 10.

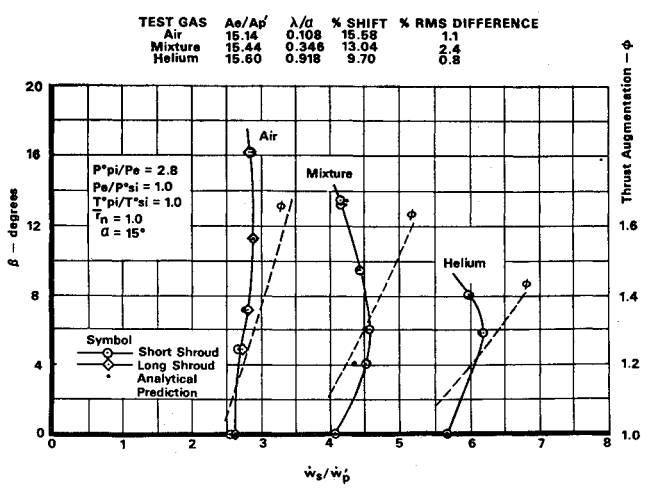

Fig. 9 Comparison of the analytical prediction with the experimental variation, pressure ratio = 2.8.

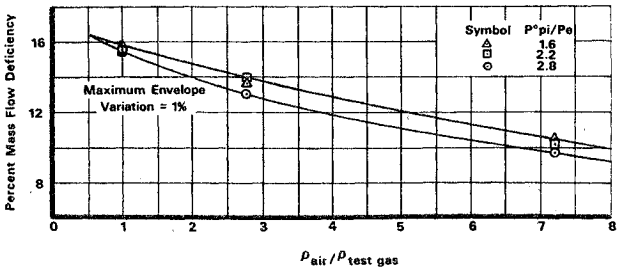

Fig. 10 Percent mass flow deficiency.

The entrainment coefficient λ for each set of analytical values illustrated in Figs. 7–9 was determined to give a minimum rms percentage difference relative to the experimental data points. As noted in the tabulation on each figure, the rms percentage difference varied from a maximum of 4% to a minimum of 0.3%.

The λ/α values yielding the minimum rms percentage differences are plotted in Fig. 11 as a function of the ratio of air density to primary gas density, for primary pressure ratios corresponding to Figs. 7–9. These variations are seen to be linear functions of the density ratio, with the slope of the variation increasing with decreasing primary pressure, and the intercepts through zero. In order to assess the sensitivity of the analytical results to the magnitude of the entrainment coefficient, this coefficient was varied and its values yielding rms percentage differences 1% greater than the minimum were determined. These results for a pressure ratio of 2.2, yield variations in the parameter λ/α from approximately $\pm 20\%$, for air as the primary gas, to around $\pm 8\%$ with helium.

Concluding Remarks

The combination of the revised jet flow analysis with associated experimentally determined values of entrainment coefficient and mass flow deficiency provides effective tools for predicting the performance of rotary jet flow inductors over a range of flow density ratios from 1:1 to 1:7 and over a range of primary ratios from 1.6 to 2.8. The concept of entrainment mixing before rather than after mutual flow deflection makes it possible to correlate the analysis with test results over the entire tested range of density ratios. The entrainment coefficient decreases somewhat with increasing primary pressure ratio and increases in proportion to the secondary to primary flow density ratio. Optimum thrust augmentation on the order of 1.35 is obtained at about 3:1 secondary to primary density ratio and 6° spin angle. The results refer to a rotary jet augmentor with a shroud exit area over primary flow area of $A_e/A_p' = 16$, the shroud having a constant inner diameter and a diameter to length ratio of about one.

When evaluating rotary jet augmentors of different geometry and operating conditions a number of questions arise. First, in practical applications the primary gas will often have higher temperature than the secondary. Unpublished tests conducted by J. L. Porter at the McDonnell-Douglas Corporation indicate that the entrainment coefficients established here are applicable also to flows with temperature differences if the appropriate density ratio in the interaction duct is used. Second, scale effects may be suspected to influence the analysis. The previously mentioned hot gas tests were conducted with about 10 times higher flow rates but otherwise similar geometry and indicate the absence of

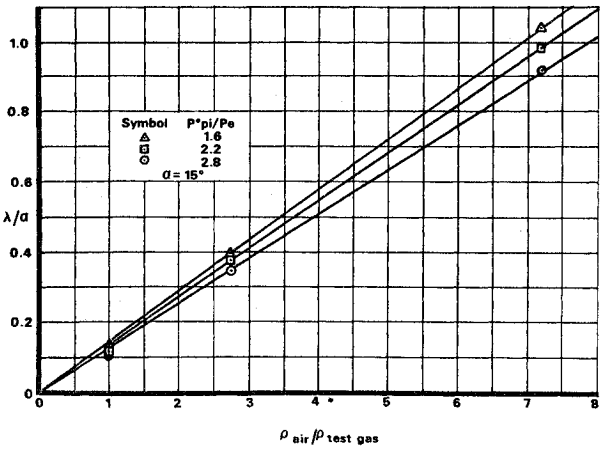

Fig. 11 Empirical variation of the entrainment parameter with density ratio.

substantial scale effects except for the greater ease to hold leakage flow through the seals down. Third, it is obvious that the values of the entrainment coefficient given here should not be used for drastically different geometry as expressed for example by the area ratio A_e/A_p'. From the experience with the tests reported by Hohenemser and Porter,[4] it would appear that the present analysis with associated empirical factors can be expected to be valid for area ratios A_e/A_p' of about 10 to 30, assuming that primary nozzle coning angle and spin angle are optimized. Fourth, one should keep in mind that the conditions tested refer to a ratio of total secondary inlet pressure to interaction duct static exit pressure of one. If this ratio is substantially higher than one, the primary to secondary inlet velocities will become less different in magnitude and a reduction in the entrainment coefficient can be expected. Fifth, primary pressure ratios higher than 2.8 may be of interest. As long as under-expanding nozzles are used, the entrainment coefficient is expected to continue to drop with increasing pressure ratios. Finally, in practical applications it may be advantageous to change the pressure in the interaction duct by a subsequent diffusor or nozzle, and the question arises if and to what degree the processes in the interaction duct can affect the efficiency of the subsequent diffusor.

References

[1] Payne, P. P., "Viscous Mixing Phenomena with Particular Reference to Thrust Augmentors," AIAA Paper 64-798, Chateau Laurier, Ottawa, Canada, 1964.

[2] De Leo, R. V. and Rose, R. E., "An Experimental Investigation of the Use of Supersonic Driving Jets for Ejector Pumps," TR 57-357, ASTIA Document AD 206662, Dec. 1958, Wright Air Development Center.

[3] Foa, J. V., "A Vaneless Turbopump," *AIAA Journal*, Vol. 1, No. 2, Feb. 1963, pp. 466–467.

[4] Hohenemser, K. H. and Porter, J. L., "Contribution to the Theory of Rotary Jet Flow Induction," *Journal of Aircraft*, Vol. 3, No. 4, July-Aug. 1966, pp. 339–346.

[5] Sarro, C. A. and Avellone, G., "A Pseudo-Blade Propulsion System for Marine Application," AIAA Paper 66-660, Colorado Springs, Colo., 1966.

[6] McBrayer, J. D., "A New Analytical Model Derived from Experimental Studies on the Energy Transfer across Moving Gaseous Interfaces," D.Sc. dissertation, Jan. 1968, Washington University, St. Louis, Mo.